



Clinically relevant mouse models of Charcot–Marie–Tooth type 2S

Paige B. Martin^{1,†}, Sarah E. Holbrook^{1,2,†}, Amy N. Hicks¹, Timothy J. Hines¹, Laurent P. Bogdanik¹, Robert W. Burgess¹  and Gregory A. Cox^{1,*} 

¹The Jackson Laboratory, Bar Harbor, ME 04609, USA

²The University of Maine, Orono, ME 04469, USA

*To whom correspondence should be addressed at: The Jackson Laboratory, 600 Main St., Bar Harbor, ME 04609, USA. Tel: +1 2072886502; Fax: +1 2072886073; Email: greg.cox@jax.org

†These authors contributed equally to the manuscript

Abstract

Charcot–Marie–Tooth disease is an inherited peripheral neuropathy that is clinically and genetically heterogeneous. Mutations in *IGHMBP2*, a ubiquitously expressed DNA/RNA helicase, have been shown to cause the infantile motor neuron disease spinal muscular atrophy with respiratory distress type 1 (SMARD1), and, more recently, juvenile-onset Charcot–Marie–Tooth disease type 2S (CMT2S). Using CRISPR–cas9 mutagenesis, we developed the first mouse models of CMT2S [p.Glu365del (E365del) and p.Tyr918Cys (Y918C)]. E365del is the first CMT2S mouse model to be discovered and Y918C is the first human CMT2S allele knock-in model. Phenotypic characterization of the homozygous models found progressive peripheral motor and sensory axonal degeneration. Neuromuscular and locomotor assays indicate that both E365del and Y918C mice have motor deficits, while neurobehavioral characterization of sensory function found that E365del mutants have mechanical allodynia. Analysis of femoral motor and sensory nerves identified axonal degeneration, which does not impact nerve conduction velocities in E365del mice, but it does so in the Y918C model. Based on these results, the E365del mutant mouse, and the human allele knock-in, Y918C, represent mouse models with the hallmark phenotypes of CMT2S, which will be critical for understanding the pathogenic mechanisms of *IGHMBP2*. These mice will complement existing *Ighmbp2* alleles modeling SMARD1 to help understand the complex phenotypic and genotypic heterogeneity that is observed in patients with *IGHMBP2* variants.

Introduction

Charcot–Marie–Tooth disease (CMT) is comprised of a broad clinicogenetic spectrum of inherited peripheral neuropathies (IPN), impacting approximately 1 in 2500 people (1). CMT is clinically segregated into two broad forms. Type 1 is characterized by demyelination and reduced nerve conduction velocity (NCV). Type 2 is characterized by axon loss and reduced action potential amplitudes. Additionally, there are intermediate forms that display both demyelination and axon loss. To date, over 80 genetic contributors to CMT have been identified, some of which are also known to contribute to motor neuron disease (MND) (2–5). This overlap of IPN and MND has recently begun to be established, with genetic contributions involved in RNA metabolism, protein homeostasis and axonal transport/maintenance being linked to both types of disease (6–8).

Variants in *IGHMBP2* have been identified in an axonal CMT, classified as CMT type 2S (CMT2S) (9,10). A mutation in *Ighmbp2* was first identified as the cause of the neuromuscular degeneration (*nmd*^{2J}) mouse mutation (11), and subsequently, variants in *IGHMBP2* were implicated in a severe infantile MND, spinal muscular atrophy with respiratory distress type 1 (SMARD1). *IGHMBP2* is a ubiquitously expressed DNA/RNA helicase that is putatively involved in RNA metabolism; its preferred substrate is GC-rich dsRNA, which it unwinds in a 5' to 3' direction (12). Growing evidence has shown that *IGHMBP2* may

also play a role in translation, as it has been found to associate with translational machinery and is predominantly located in the cytoplasm (12,13). Both CMT2S and SMARD1 are autosomal recessive with missense and/or truncating variants (9,10,14,15). While SMARD1 patients present within the first few months of life, CMT2S patients typically present after one year of age without respiratory involvement (9,10,14,15).

To date, only the *nmd*^{2J} mouse model, on both the C57BL/6J and the FVB/NJ backgrounds (16–18) and the *Ighmbp2*-D564N, on the FVB/NJ background (19), have been described as SMARD1 models. Here we present work highlighting the generation and characterization of the first CMT2S mouse model C57BL/6J-*Ighmbp2*^{em1Cx}/Cx (E365del) and the first human CMT2S allele knock-in model C57BL/6J-*Ighmbp2*^{em5Cx}/Cx (Y918C). Phenotypic and neurobehavioral assessment indicates that the mice display progressive sensory and motor function deficits and axon degeneration. These mice provide a critical resource for future pathomechanistic and preclinical validation work.

Results

CRISPR–cas9 induced *Ighmbp2*–E365del mutation and human knock-in allele *Ighmbp2*–Y918C

During the course of a CRISPR–cas9 mutagenesis project to produce new alleles of *Ighmbp2* in mice, a founder carrying a novel

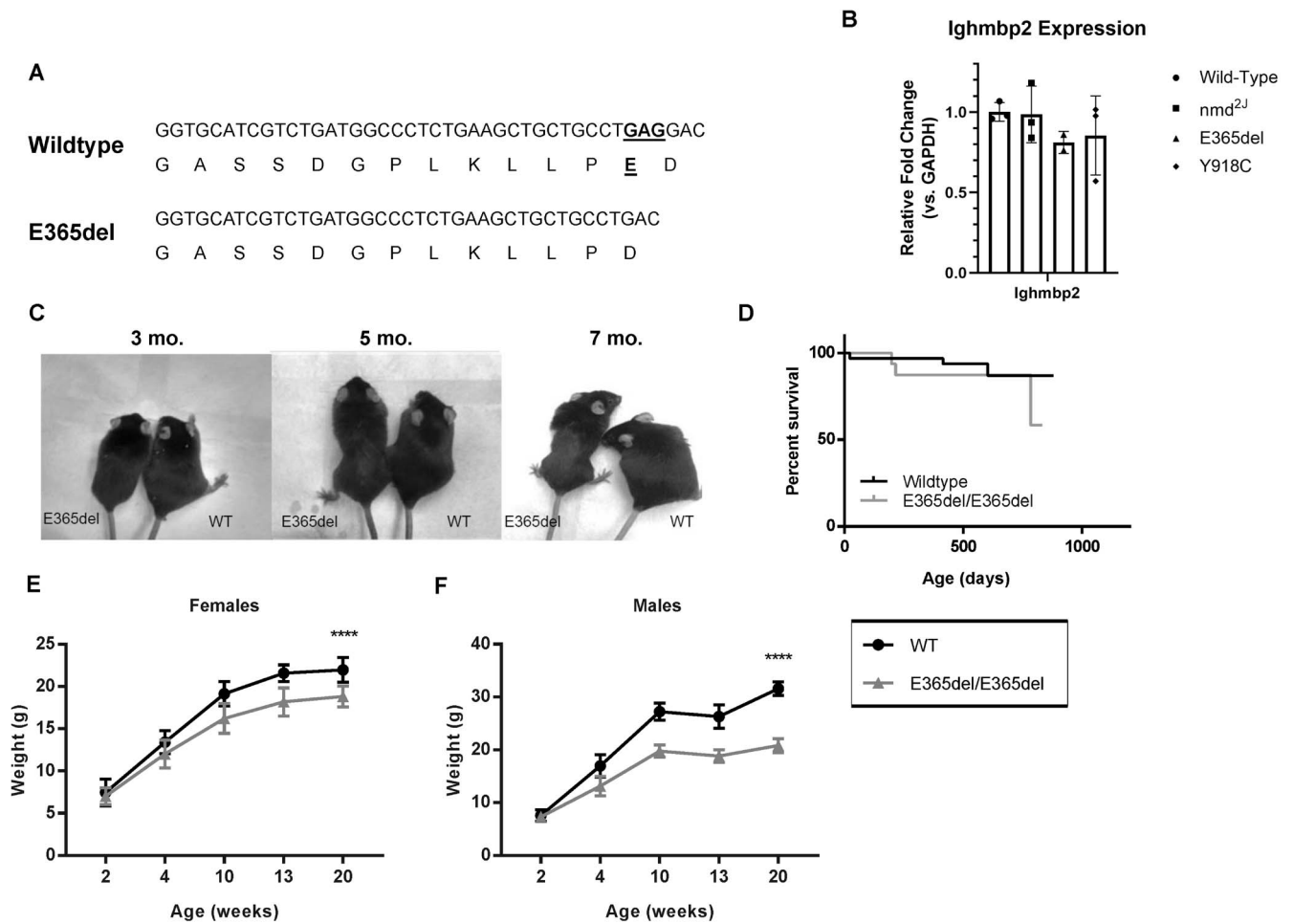


Figure 1. CRISPR-cas9 induced E365del IGHMBP2 variant. **(A)** Schematic of the variant in the *Ighmbp2*^{em1} strain (c. 1093_1095del; p.Glu365del) three nucleotide deletion underlined in the WT allele. **(B)** *Ighmbp2* mRNA expression in 2-week-old WT, *nmd2J*, E365del and Y918C HOM mutant spinal cords normalized to GAPDH ($n = 3$ WT, $n = 2$ E365del, $n = 3$ *nmd2J*, $n = 3$ Y918C). **(C)** Comparison of HOM and WT littermates at 3, 5 and 7 months indicates a progressive wasting of the muscles in the hindlimbs and waist, which is most remarkable at 7 months of age. **(D)** Survival curve of WT mice and E365del HOM showed no significant difference between the two ($n = 33$ WT, $n = 26$ HOM, $P = 0.4704$; Log-Rank, Mantel-Cox test). **(E)** and **(F)** HOM E365del mice had significantly reduced body weight, evident by 10 weeks of age ($P < 0.0001$) in females and by 4 weeks of age in males ($P < 0.0001$). Mean body weights \pm SD are shown for HOM and WT littermates ($n = 4$ – 15 mice per time point).

deletion in exon 8 (c.1093_1095del; p.Glu365del), within the helix domain of *Ighmbp2*, was identified (Fig. 1A). This variant is predicted to delete a single amino acid while maintaining the reading frame, but does not significantly impact transcript levels of *Ighmbp2* (Fig. 1B).

Ighmbp2-E365del homozygous mice have functional sensory and motor deficits

Initial characterization of the homozygous (HOM) E365del mutants found that mice was presented as thin, wasted and with paresis of the hind quarters, first notable by 2–3 months of age, and progressing over time (Fig. 1C). While the mice have an overt hindlimb muscular atrophy, this does not impact their overall survival (Fig. 1D), but does result in reduced body weight over time in the mutant mice (Fig. 1E and F). Extensive characterization of E365del HOM mutants indicated progressive muscular wasting and motor deficits, similar to IGHMBP2-associated CMT2S patients (9,10,14,15). To validate the E365del mutant as a CMT2S disease model, we analyzed clinically relevant phenotypes. Mice were tested through a battery of neurobehavioral and physiological assessments at separate time points to assess

sensation (von Frey, adhesive removal, hot plate), muscle strength and motor function (grip strength, rotarod, voluntary running wheel) and peripheral nerve function and morphology (NCV, nerve histology) (Supplementary Material, Fig. S1).

CMT2S patients exhibit a distal sensory loss that spreads proximally as the disease progresses (9,10,14,15). To determine if HOM mice had sensory deficits, we used the von Frey assay to test for mechano-sensitivity, and hot plate to test for thermo-nociception. HOM mutant mice exhibited an increase in sensitivity to mechanical force (allodynia) compared with wild-type (WT) mice apparent by 12 weeks of age (Fig. 2A). There is a somewhat reduced thermo-sensitivity between genotypes when all time points are grouped together, but does not appear at each time point, respectively (Fig. 2B).

As patients of CMT2S present with both sensory and motor phenotypes, we also used an assay to test for sensorimotor deficits. The adhesive removal test uses a sticker placed on the mouse's forehead between the eyes and tests sensation and dexterity by measuring the time it takes to remove the adhesive. HOM mutant mice take longer to remove the adhesive compared with their WT littermates (Fig. 2C).

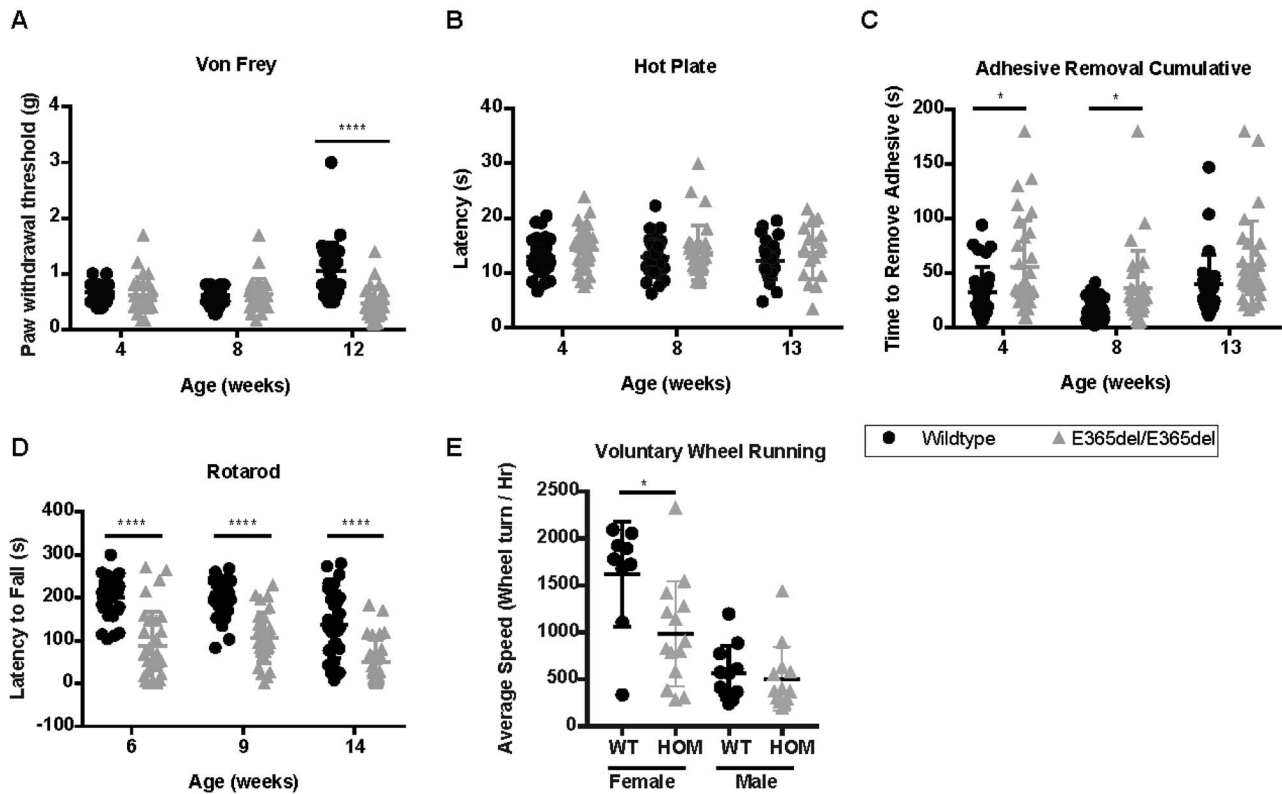


Figure 2. E365del HOM mice model sensory and motor deficits. (A) von Frey assessment indicated that HOM mice had significant ($P < 0.0001$) hypersensitivity to mechanical allodynia. HOM sensitivity was $(0.47 \pm 0.3 \text{ g}, n = 30)$ evident by 12 weeks of age compared with WT ($1.0 \pm 0.5 \text{ g}, n = 30$) littermates, which was not apparent at 4 or 8 weeks of age in WT ($0.665 \pm 0.184, n = 26$; $0.610 \pm 0.174, n = 26$) or HOM ($0.619 \pm 0.314, n = 30$; $0.624 \pm 0.289, n = 30$). Individual threshold data points with mean and SD are plotted. (B) Hot plate assay was utilized to test for deficits in thermo-nociception. HOM mice show a genotype dependent sensitivity across the tested time-points ($P = 0.0193$). Individual latency times with mean and SD are plotted. (C) Adhesive removal assay used for sensorimotor deficits indicated that HOM mice took significantly longer to remove the sticker from the forehead across the tested time-points ($P < 0.0001$). At 4 and 8 weeks of age this difference was pronounced ($P = 0.0162, P = 0.0226$); however, by 13 weeks of age there was no significant difference ($P = 0.0889$). Individual removal times with mean and SD are plotted. (D) Motor performance on a rotarod was measured by latency to fall and indicated significant deficits in HOM mice evident by 6 weeks of age ($P < 0.0001$). Individual latency times with mean and SD are plotted. (E) Motor performance and endurance was tested with voluntary running wheel. Average speed (total wheel rotations in dark cycle/time of dark cycle (12 h) at 15 weeks of age. WT females ($n = 9, 1621 \pm 561.8$) ran significantly faster than HOM female littermates ($n = 14, 986.8 \pm 558.6, P = 0.0158$), while HOM males ($n = 13, 505.4 \pm 341.1$) did not show significant differences from WT littermates ($n = 11, 571 \pm 376.6, P = 0.4940$). Mann-Whitney test, individual speed averages with mean and SD are plotted. For (A)–(D) assays $n = 18$ – 30 mice per time-point, males and females were not significantly different and were therefore combined.

CMT2S patients miss critical developmental motor milestones and may need walking aids in order to be ambulatory owing to locomotor deficits (9,10). Therefore, we analyzed locomotor performance of the E65del HOM mice. HOM mice exhibited reduced performance on the accelerating rotarod, a test of muscular endurance, balance and motor coordination (Fig. 2D). We additionally tested motor endurance and function with a voluntary running wheel. Female HOM mice had a slower overall speed during the dark cycle period (when mice are active) than their WT littermates, while male mice, overall less active regardless of genotype, exhibited no difference (Fig. 2E).

Progressive degeneration of femoral sensory and motor myelinated axons and neuromuscular junctions in E365del HOM mice

To determine if the sensory and motor phenotypes described before are indeed neurogenic, as observed in CMT2S patients, we assessed the function and morphology of peripheral nerves. For this, we analyzed the femoral sensory and motor nerves from the mice after undergoing the neurobehavioral assessments, cohorts of which are outlined in Supplementary Material, Figure S1.

Degeneration of myelinated sensory axons was apparent by 4 weeks of age, with about 50% loss by 20 weeks of age (Fig. 3A and B). Motor axon degeneration was apparent by 10 weeks of age, with an approximately 30% reduction by 20 weeks of age (Fig. 3C and D). The neurodegeneration in the femoral sensory nerves impacted all axon calibers except for a small population of axons larger than $6 \mu\text{m}$ (Fig. 3E). The neurodegeneration in the femoral motor nerves significantly impacted axon calibers between 2 and $8 \mu\text{m}$ but not the smallest axons between 0 and $2 \mu\text{m}$ and those $>8 \mu\text{m}$ (Fig. 3F). An assay of nerve function was consistent with an entirely axonal neuropathy, as nerve conduction velocities (NCV) were not different between HOM mice and WT's littermates (Fig. 3G).

To determine if there is a dose-dependent effect of the phenotype based upon the number of mutant alleles the animal is carrying, the same analyses were performed in parallel in heterozygous E365del mice (Supplementary Material, Fig. S1, cohort 1). No differences from controls were identified (Supplementary Material, Fig. S2) indicating that the phenotypes described in HOM E365del animals were completely recessive. This is consistent with heterozygous carriers of IGHMBP2/CMT2S alleles being asymptomatic.

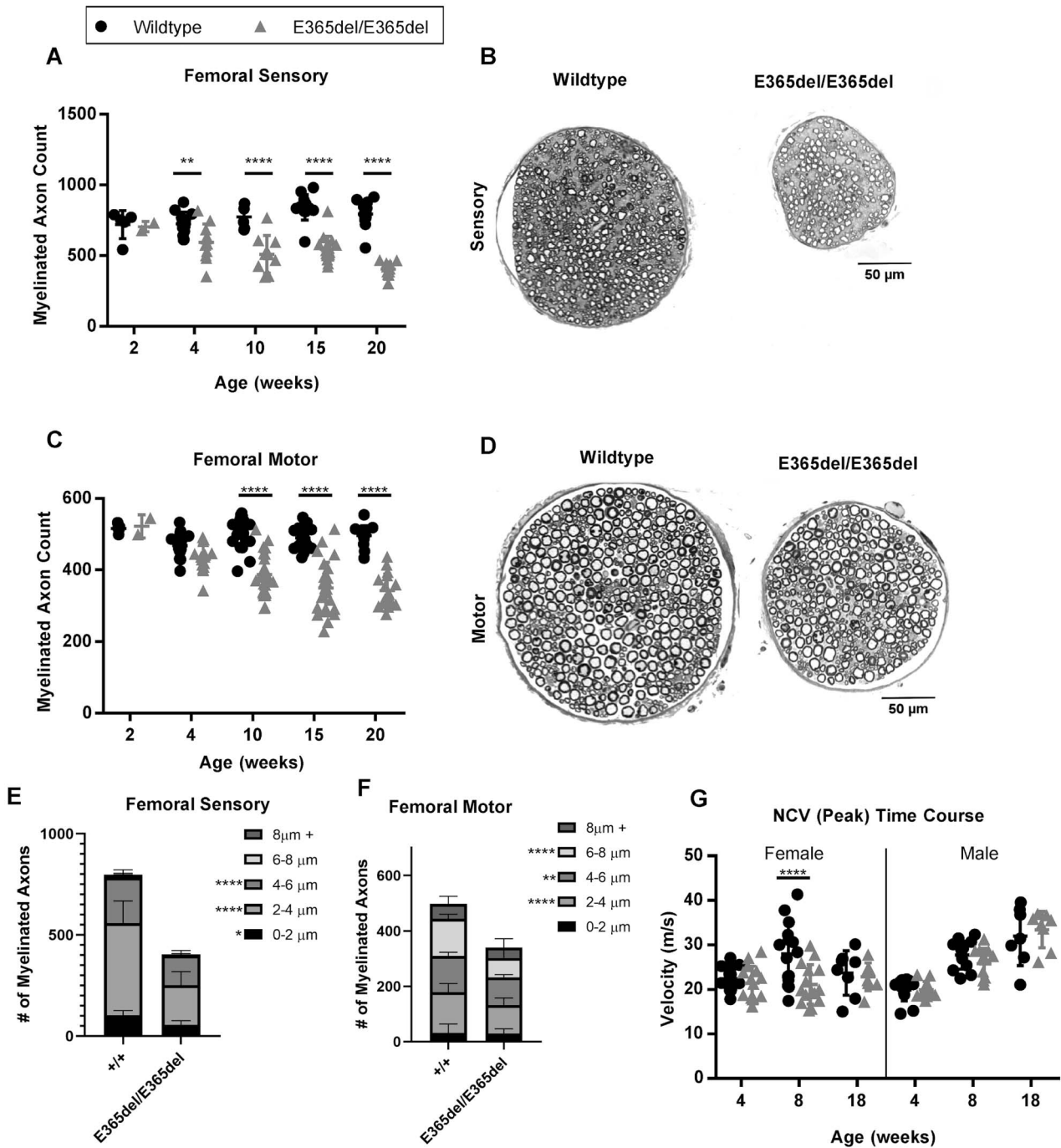


Figure 3. E365del HOM mutants displayed progressive degeneration of femoral motor and sensory axons. **(A)** Quantification of myelinated axons in the femoral sensory branch at five time points between 2 and 20 weeks indicates a significant loss evident by 4 weeks of age ($P=0.0083$) with about a 50% overall reduction in the HOM sensory axons (404 ± 50 , $n=11$) compared with WT (794 ± 96 , $n=12$) by 20 weeks of age. **(B)** Cross-section of the WT femoral sensory branch is larger with more myelinated axons than the HOM sensory branch at 20 weeks of age. **(C)** Quantification of myelinated axons in the femoral motor branch at five time points between 2 and 20 weeks indicates a significant loss evident by 10 weeks of age ($P=0.0001$) with about a 31% overall reduction in the HOM motor axons (342.3 ± 47 , $n=16$) compared with WT (496 ± 28.3 , $n=15$) by 20 weeks of age. **(D)** Cross-section of femoral motor branch for WT indicated a significantly larger overall size with more myelinated axons. **(E)** Axon diameters of the femoral sensory nerves were analyzed via the Sidak's multiple comparison's test, and found that in bin sizes 0-2 μ m, 2-4 μ m and 4-6 μ m, there were significantly fewer axons in homozygotes than WT mice (0-2 μ m, +/+ = 103.5 ± 22.53 , E365del/E365del = 55.82 ± 20.65 , $P=0.0177$, 2-4 μ m, +/+ = 455.3 ± 109.5 , E365del/E365del = 196 ± 66.67 , $P \geq 0.0001$, 4-6 μ m, +/+ = 225.2 ± 37.87 , E365del/E365del = 147.5 ± 23.93 , $P \geq 0.0001$). +/+, $n=12$, E365del/E365del, $n=12$). **(F)** Axon diameters of the femoral motor nerves were analyzed via the Sidak's multiple comparison's test, and found that in bin sizes 2-4 μ m, 4-6 μ m and 6-8 μ m there were significantly fewer axons in homozygotes than WT mice (2-4 μ m, +/+ = 146.2 ± 31.43 , E365del/E365del = 102.9 ± 25.69 , $P \leq 0.0001$, 4-6 μ m, +/+ = 131.8 ± 12.69 , E365del/E365del = 100.5 ± 9.585 , $P \geq 0.0026$, 6-8 μ m, +/+ = 133.6 ± 16.17 , E365del/E365del = 70.19 ± 29.48 , $P \leq 0.0001$). +/+, $n=13$, E365del/E365del, $n=16$). **(G)** NCV was significantly reduced in only female mice at 8 weeks of age ($P < 0.0001$), but by 18 weeks of age NCV was not significantly reduced in either male or female mice.

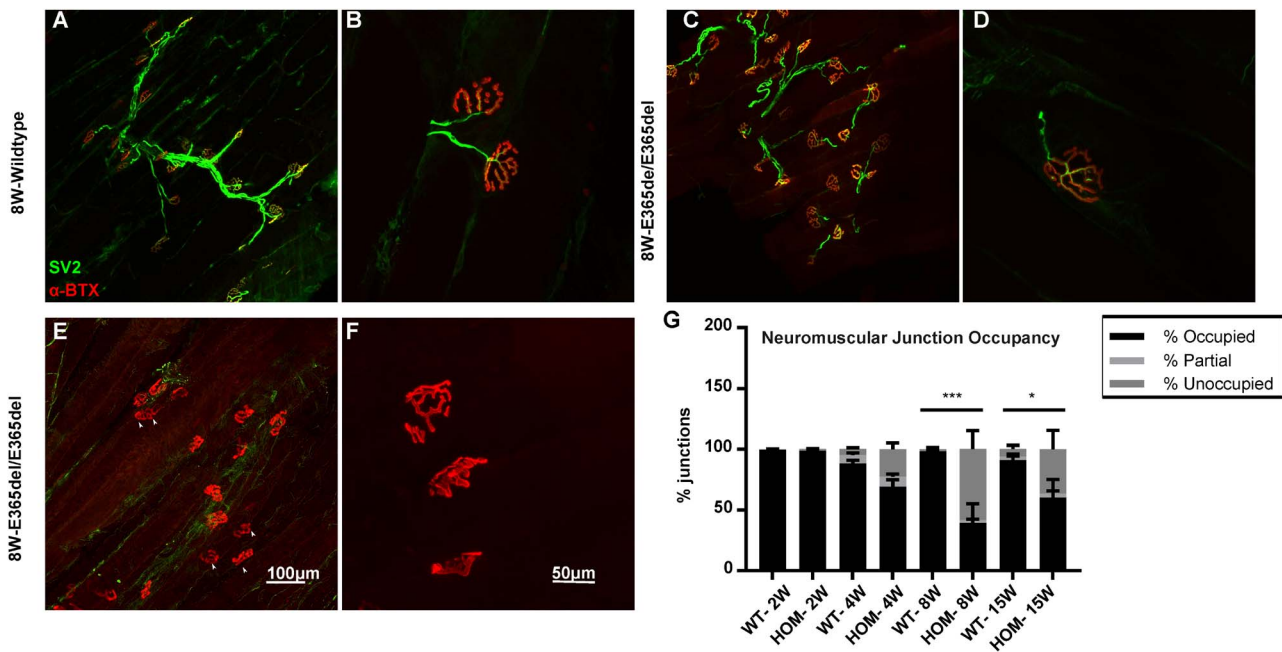


Figure 4. NMJ degeneration in the E365del HOM mice. (A) and (B) NMJs of MG muscle from 15 week-old WT mice. Tissues were stained for presynaptic vesicles (anti-SV2), neurofilaments (anti-neurofilament 2H3) and acetylcholine receptor (α -bungarotoxin). (A) low magnification and (B) high magnification. (C) and (D) HOM mice have exhibited a spectrum of phenotypes with some areas had many innervated NMJs. (E) and (F) While other HOM mice had many denervated NMJs highlighted with white arrows. (G) NMJs were quantified as occupied, partially occupied or unoccupied. The percent of junctions that were unoccupied was significantly different in HOM compared with WT evident by 8 weeks of age ($P = 0.0006$) ($n = 3-20$ per time point). Scale bar in (E) applies to (A), (C), scale bar in (F), applies to (B), (D).

Since CMT2S causes a distal loss of motor and sensory axons, we examined the neuromuscular junctions (NMJs) of HOM and WT mice. In the gastrocnemius muscle of 15-week-old WT mice, each muscle fiber is contacted by a motor nerve terminal, which completely overlaps the postsynaptic acetylcholine receptors (Fig. 4A and B). However, in the HOM E365del mice, the presynaptic terminal is often absent, with regions of postsynaptic receptors present without complete innervation of the junction (Fig. 4C-F). When the percent of completely denervated junctions was quantified we observed a significant and progressive loss of innervation evident by 8 weeks of age (Fig. 4G, Supplementary Material, Fig. S3). NMJ loss is more severe than the femoral motor nerve axon loss. The deficits at the NMJ are more pronounced than the femoral motor axon loss. This discrepancy could be explained by the lag time between NMJ degeneration and the resulting axon degeneration, and suggests a dying-back mechanism is occurring.

Muscular weakness and atrophy in E365del HOM mice

As the NMJs were significantly denervated by 8 weeks of age, we analyzed the impact on the distal hindlimb muscles. Muscular strength of the limbs was tested using a standard grip strength assay, analogous to grip strength measures utilized in human patients, which is reduced in CMT2S patients (17). To tease apart the contribution of the forelimbs and hindlimbs to the phenotype, we examined the strength of the forelimbs alone, as well as all limbs combined. At all time-points tested, HOM mice exhibited a reduction in all-paw grip strength compared with WT littermates, for both male and female mice (Fig. 5A). However, we found that the reduction was more pronounced in the all-paw grip than the forepaws alone (Supplementary Material, Fig. S4A), suggesting that IGHMBP2 E365del variant impacts the hindlimbs

more than the forelimbs. Likewise, an assessment of lower limb muscular strength, isometric force-frequency curves, found progressive muscular weakness with age (Supplementary Material, Fig. S5).

Analysis of the histology of the medial gastrocnemius (MG) shows regions of atrophic fibers indicative of neurogenic atrophy in the HOM MG compared with uniform fibers in the WT muscle (Fig. 5B and C, Supplementary Material, Fig. S4B). Muscle weights of triceps surae (MG, lateral gastrocnemius and soleus) also show significant differences in muscle weight to body weight ratios by at least 4 weeks in males (Fig. 5D). This muscle atrophy was widespread, as indicated by an overall smaller hindlimb cross-section size (Supplementary Material, Fig. S4C).

Previous work has shown that cardiac muscle, as well as skeletal muscle, can be impacted by variants in *Ighmbp2* (13,20). In order to determine if the CMT2S model has phenotypes of dilated cardiomyopathy, we assessed the heart rate, EKG parameters and heart size. None of the assessed measures were indicative of cardiac dysfunction or abnormal phenotype owing to the E365del variant (Supplementary Material, Fig. S6). Additionally, we determined that neuronal expression of WT *Ighmbp2* using a transgene driven by the rat neuron-specific enolase 2 (NSE Tg) promoter in the E365del HOM mice makes them indistinguishable from WT animals (Fig. 6A-E). Unlike the previously characterized neuron-specific rescue in the SMARD1 mouse model (*nmd^{2l}*) using this same transgene (20), neuron-rescued E365del HOM mice did not show signs of secondary skeletal or cardiac myopathies (Fig. 6F).

CMT2S patient allele IGHMBP2-Y920C validated in mouse model

While the E365del HOM mouse recapitulates many of the clinical features observed in CMT2S patients, this is not a variant that has yet been observed in the patient population. Therefore, to further

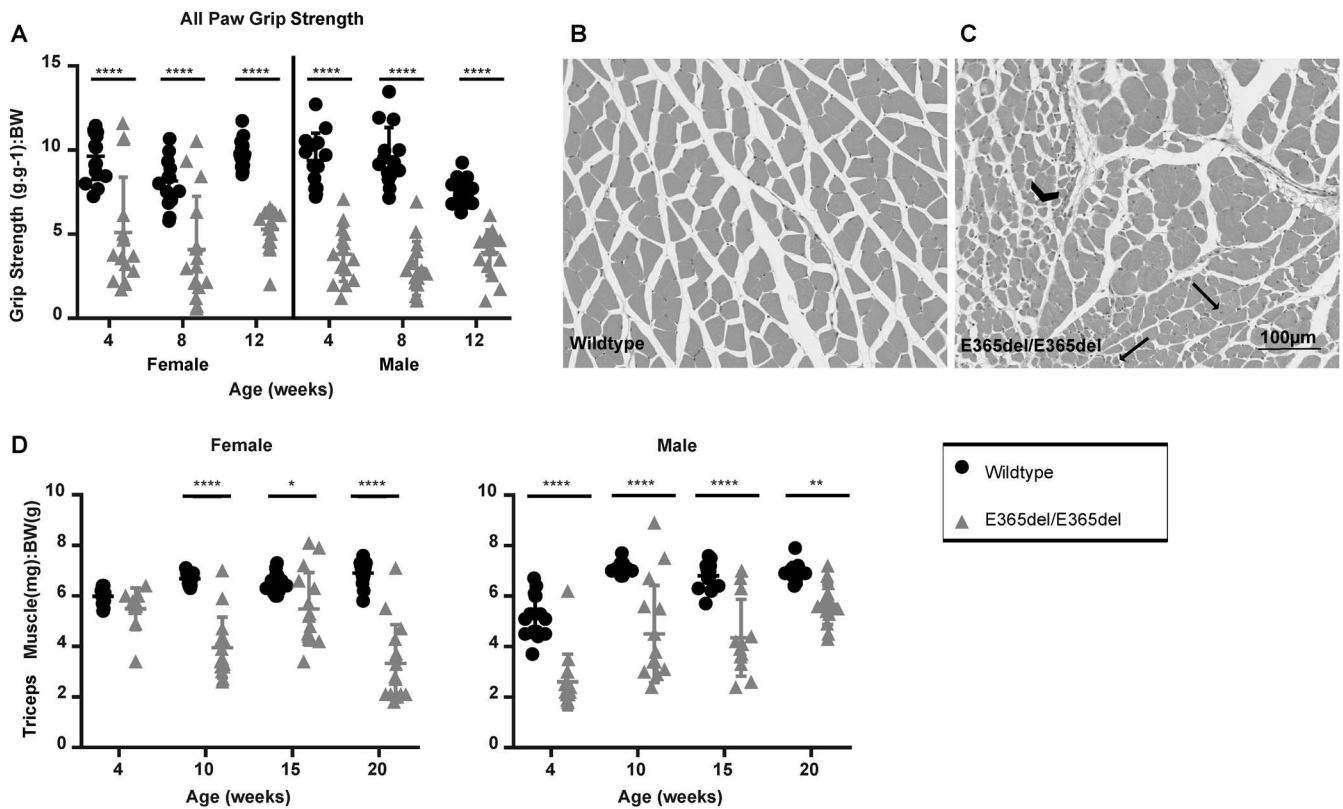


Figure 5. E365del mice show muscle weakness and neurogenic atrophy. (A) All-paw grip strength assessment indicated that HOM mice were weaker than WT at all time points ($P < 0.0001$) for both female and male. Individual data points with mean and SD shown. (B) 8 week of age WT MG cross-section stained with hematoxylin and eosin. (C) HOM MG cross-section shows regions of atrophied alongside regions of larger area fibers highlighted with an arrow head, with few central nuclei fibers highlighted by black arrows. (D) Both female and male HOM mice exhibited a difference in the triceps muscle to body weight ratio, evident by 10 weeks of age ($P < 0.0001$) in females and 4 weeks of age in male ($P < 0.0001$). Individual data points with mean and SD shown.

broaden the spectrum of CMT models available, we generated a human allele knock-in (human: c.2759A>G, p.Tyr920Cys; mouse c.2753A>G, p.Tyr918Cys). The patient carrying this HOM variant is described as presenting with a juvenile-onset CMT with mild motor and sensory deficits (21).

Similar to our E365del HOM mice, our mouse model Y918C, modeled after the p.Tyr920Cys human variant, also presents with mild hindlimb wasting (Fig. 7A), decreased body weight in males and females (Fig. 7B and C) and deficits in motor function, apparent by inverted wire hang testing starting at 3 weeks of age (Fig. 7D). Like both the human CMT2S patients and the E365del mouse model, the Y918C mouse model does not significantly impact lifespan to at least 8 months of age (Fig. 7E).

To determine if the sensory and motor axonal degeneration that is present in the E365del model were also observable in the Y918C model, we assessed the morphology and functional properties of the peripheral nerves. At 8 weeks of age we observed degeneration of myelinated axons in HOM mice, with an approximately 13% overall reduction in the sensory branch and a 34% overall reduction in the motor branch of the femoral nerve (Fig. 8A–C). At 16 weeks, there is an approximately 21% reduction in the sensory branch and a 32% reduction in the motor branch, showing that most of the neuron death has occurred by 8 weeks and plateaus thereafter (Fig. 8D and E). Another difference is that, unlike the E365del, NCV testing found a decrease in velocity of the HOM and heterozygous mice compared with WT littermates (Fig. 8H), consistent with the human patient (21).

NMJs were quantified as occupied, partially occupied or unoccupied. The percent of junctions that were unoccupied was significantly different in HOM compared with WT mice at 16 weeks of age ($n = 5-7$ per time point, $P \leq 0.0001$) (Fig. 8I).

Though characterized in less detail, the Y918C mice show a slightly more severe CMT2S phenotype compared with the E365del mice. They have smaller hindlimbs, smaller motor neuron axon diameters and less occupied NMJs with approximately 30% fewer occupied NMJs at the 16-week time point compared with the E365del mice ($P = 0.0043$). However, E365del mice shows significantly more axonal loss in both motor and sensory nerves compared with Y918C (Figs 3A and C and 8B and E). As the first precise human CMT2S allele knock-in, these mice provide both construct and face validity for subsequent preclinical studies. Axonal degeneration and muscular atrophy findings were comparable to the E365del model at a similar time-point; however, at 8 weeks of age Y918C HOM mice show a clear decrease in NCV, as observed in the CMT2S patient (21). Interestingly, although Y918C and E365del mice indicate a purely recessive phenotype for almost all measures tested, Y918C heterozygous mice also show an intermediate decrease in NCV (Fig. 8H). Though decreased motor axon diameter may account for a decrease in NCV in Y918C HOM mice, there is no significant difference between Y918C heterozygous and WT mice in femoral axon caliber (Fig. 8F and G) or myelin g-ratios (Fig. 8J) to account for this decrease in NCV. E365del also shows a decrease in axon caliber, but show no abnormal NCV phenotype. However, for NCVs, the sciatic nerve was measured that is composed of a multitude of axons innervating different muscles,

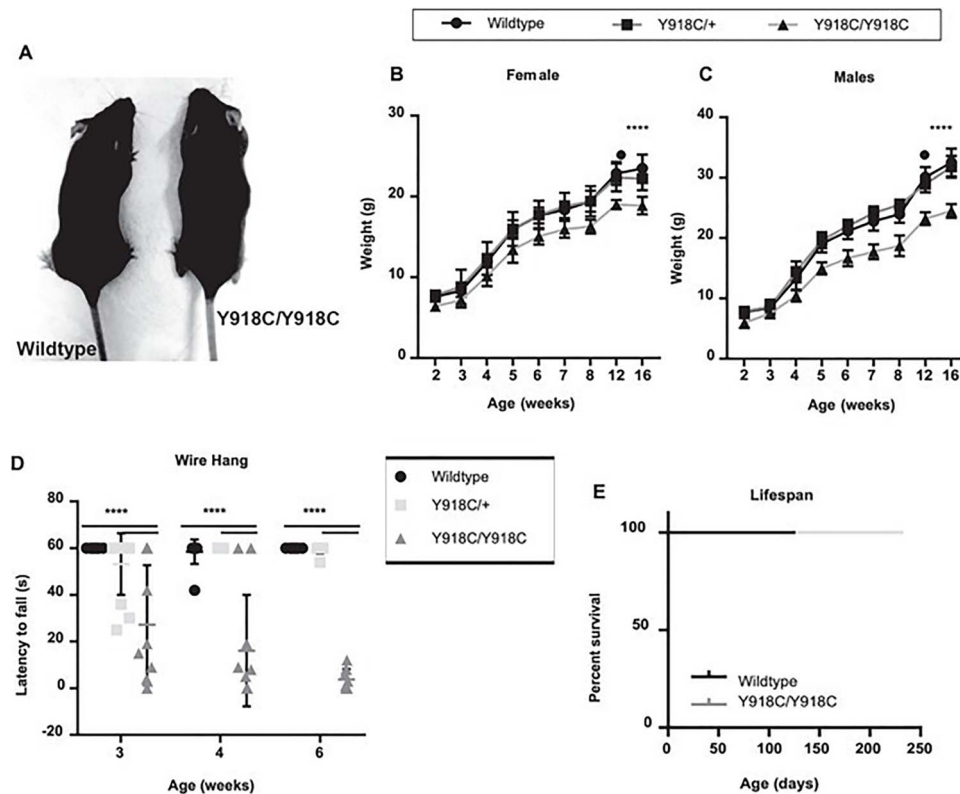


Figure 6. E365del HOM mice are rescued with neuronal expression of *Ighmbp2*. (A) 8-month-old HOM E365del mice are thin and wasted, while the e365del HOM mice carrying the *Ighmbp2*-NSE transgene are indistinguishable from WT littermates. (B) The lifespan of the *Ighmbp2*-NSE rescued E365del HOM mice is not significantly different from the E365del HOM mice ($P=0.1265$; Log-Rank, Mantel-Cox test). (C) Growth curves of female control, E365del HOM with the NSE transgene and E365del HOM shows no significant difference between NSE rescued and controls (Two-way ANOVA, $P=0.0986$), while E365del HOM with NSE have an increased growth curve compared with the E365del HOM ($P < 0.0001$; Two-way ANOVA). (D) Male E365del HOM with NSE rescued had shifted growth curves to male control mice (Two-way ANOVA, $P < 0.0001$), apparent by 32 weeks of age (Sidak's multiple comparisons test, $P=0.0008$). While they had an improved curve when compared with E365del HOM mice (Two-way ANOVA, $P < 0.0001$), apparent by 7 weeks of age (Sidak's multiple comparisons test, $P=0.0073$). (E) Femoral motor and sensory nerves showed overall size and counts to be comparable to WT myelinated axons at 8 months of age (scale bar = $50 \mu\text{m}$). (F) 8-Month-old Hematoxylin & Eosin stained skeletal (MG and soleus) and Trichrome stained cardiac muscles of E365del HOM with NSE transgene taken at $40\times$ magnification (scale bar = $5 \mu\text{m}$).

while the femoral motor nerve consists of a small subset of motor neurons examined for histopathology. This may contribute to discrepancies in NCVs and histopathology between the Y918C homozygotes, heterozygotes and WTs as well as the differences we see between Y918C and E365del. Such findings may indicate a clinically subthreshold reduction in conduction velocity, which may be present but untested in carriers. To further support this, heterozygous mice with an *Ighmbp2*-knock-out allele (IMPC) show deficits in vertical rearing activity (<https://www.mousephenotype.org/data/genes/MGI:99954>). Additional testing of *IGHMBP2* variant carriers for susceptibility of mild CMT or neuromuscular disease phenotypes is needed.

Discussion

Here we have characterized the first animal models of CMT2S. As with the human patients, the variants are recessive and causative of juvenile-onset distal axonopathy with deficits in locomotor and sensory function. The mice demonstrate progressive axonal degeneration in both the peripheral motor and sensory nerves. Like the patients, these models have a relatively unaffected lifespan, and no indications of respiratory distress. Furthermore, clinically relevant assays show that mutant mice have deficits in mechano and thermal sensation, as well as muscular strength and endurance. Based on the phenotypic similarities, these

variants are valid models of CMT2S for use in future mechanistic and preclinical studies.

The phenotypic variability observed across the *IGHMBP2*-associated disease spectrum remains poorly understood. Research examining the stability and function of patient variants suggests that both SMARD1 and CMT2S are caused by loss-of-function alleles (12,22). Variant heterogeneity alone cannot account for the phenotypic differences noted in patients, as patients with identical allelic combinations have presented with severity on both ends of the spectrum (22–24). Some work suggests that there is a possible correlation between protein expression level, helicase activity and disease severity, as a gradient of expression seems correlative with phenotype severity (22). This spectrum can be observed in the mouse models of *Ighmbp2*, as HOM null mice die at birth (data not shown and <https://www.mousephenotype.org/data/genes/MGI:99954>), and *nmd^{2j}*, which has a unique variant impacting splicing of *Ighmbp2* that results in only $\sim 20\%$ WT protein expressed, live a median lifespan of 91.5 days (11,16). Our models E365del and Y918C are both phenotypically less severe, suggestive of a hypomorphic protein, similar to that predicted in many of the patient alleles (12). The E365del variant falls within helicase domain 1C, while Y918C falls within the C terminus domain, a region that has been found to increase RNA-binding affinity (25). Both regions are critical for the enzymatic function of the helicase. An additional hypothesis in phenotypic heterogeneity is derived from work in mouse models, as well as findings in siblings,

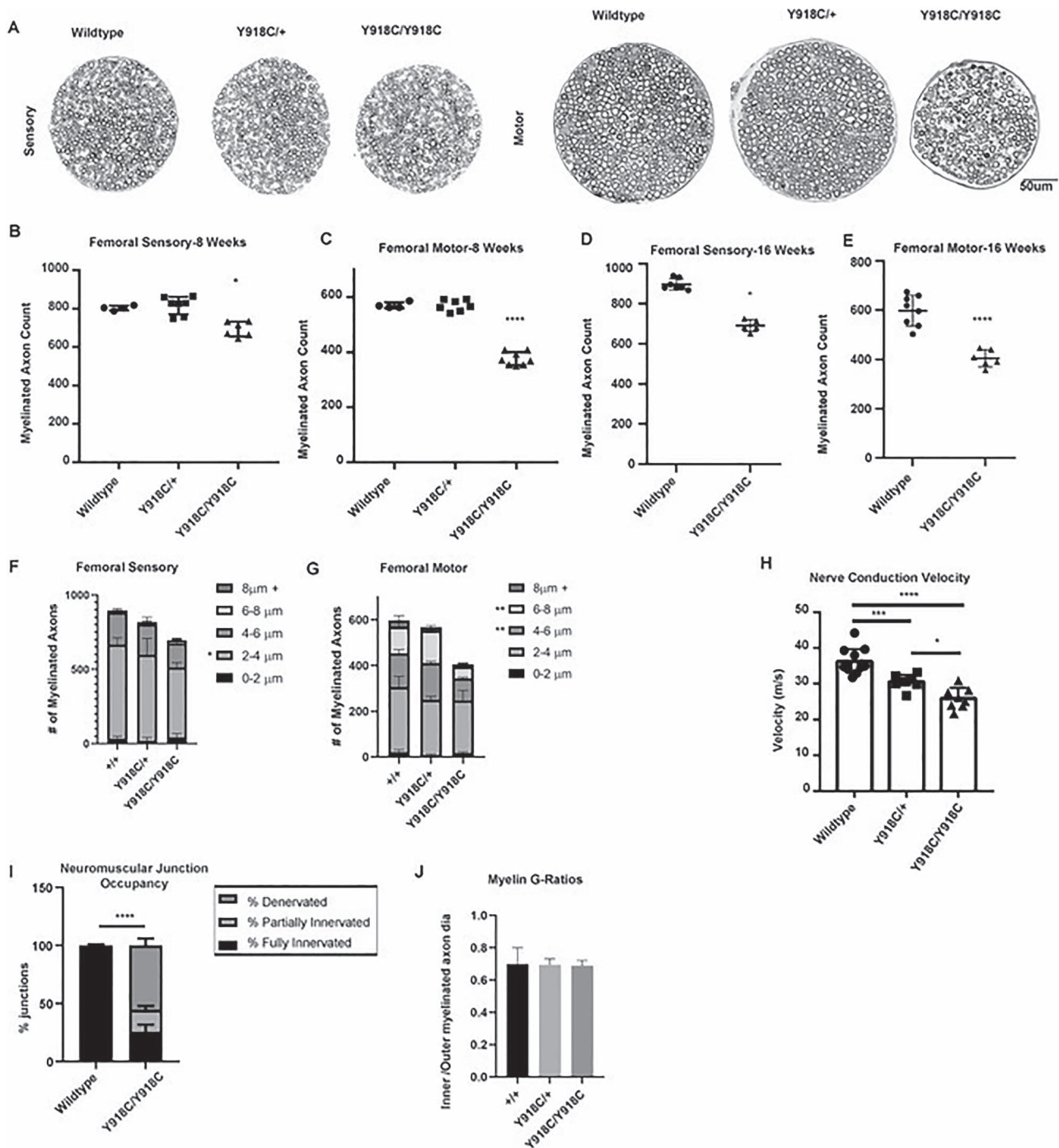


Figure 7. Y918C mice displayed decreased body weight and motor deficits. (A) Comparison of WT and HOM Y918C littermates body morphology at 2 months shows a progressive wasting of the muscles in the hindlimbs and waist in the mutants. (B) HOM Y918C mice had significantly reduced body weight, evident by 4 weeks of age ($P < 0.0001$) in females and (C) by 5 weeks of age in males ($P < 0.0001$). Mean body weights \pm SD are shown for HOM, heterozygous and WT littermates ($n = 4-15$ mice per time point). (D) HOM Y918C ($n = 10$) mice displayed deficits in motor function and endurance as tested by the inverted wire hang assay evident by 3 weeks of age compared with WT ($n = 12$) and heterozygous ($n = 13$) littermates ($P < 0.0001$). (E) Survival curve of WT mice and Y918C heterozygous and HOM showed no significant difference between ($n = 12$ WT, $n = 29$ Heterozygous, $n = 11$ HOM, $P = 0.999$; Log-Rank, Mantel-Cox test).

which suggests that genetic background variants can impact phenotypic severity (11,17,23). Future work will look to leverage our new CMT2S mouse models in identifying susceptibility to known genetic modifiers of *Ighmbp2*-associated neuromuscular disease as well as gene therapy treatment strategies.

Previous work with the *nmd^{2j}* model by our group indicated that rescuing the MND, either through neuron-specific *Ighmbp2*

expression, or genetic modification, unmasked a cardiomyopathy (13,20). We did not observe cardiac phenotypes in the E365del mice, but whether that reflects the reduced severity of the mutation compared with *nmd^{2j}*, or if there is an allelic difference in the disease mechanism, is uncertain. The basis for the cardiomyopathy in the *nmd^{2j}* mice is unclear, and it is unknown if SMARD1 and CMT2S patients are susceptible to cardiac dysfunction. This

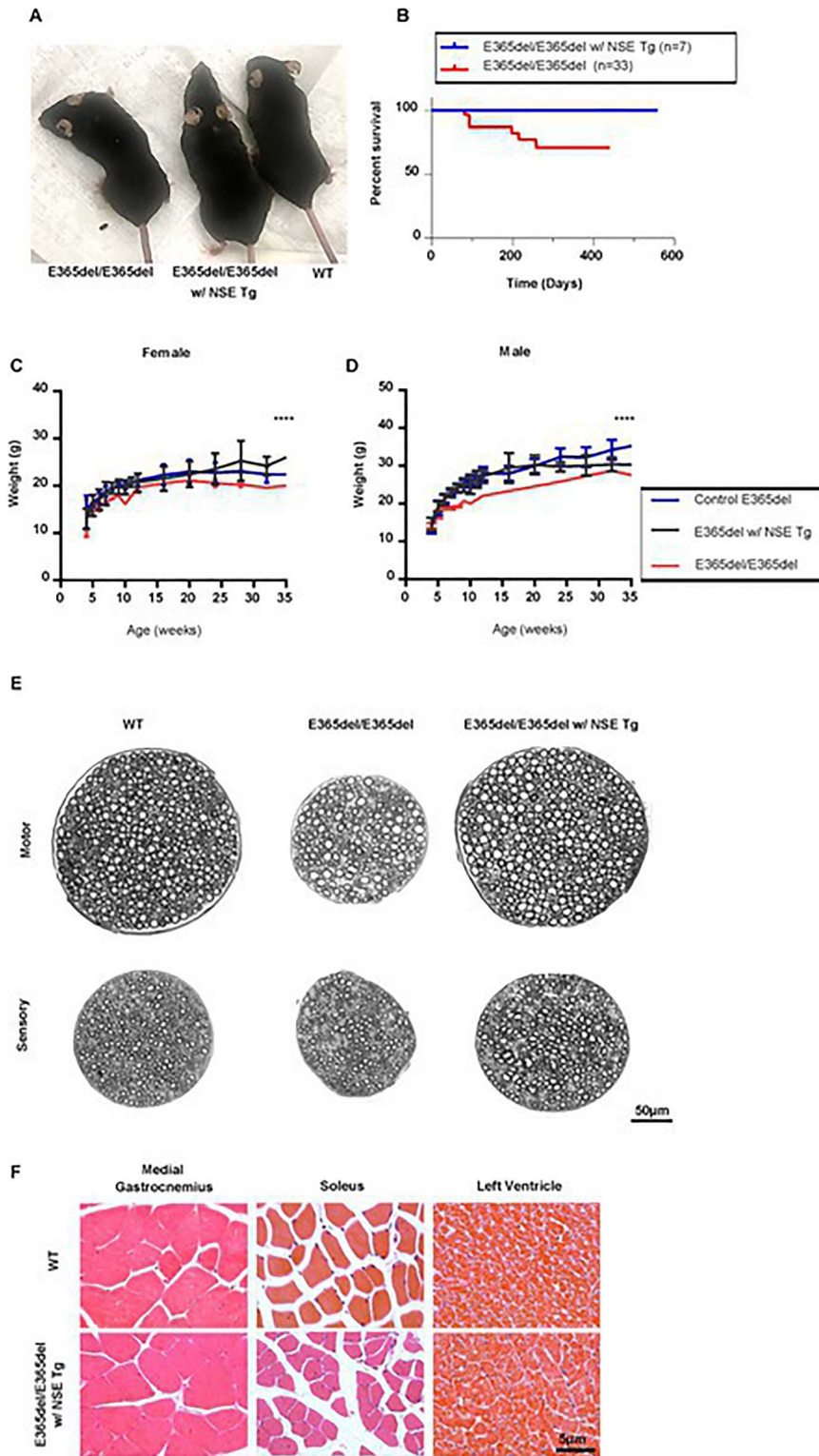


Figure 8. Y918C mice displayed degeneration of femoral motor and sensory axons. **(A)** Cross-sections of the WT, heterozygous and HOM femoral sensory and motor branches at 8 weeks of age. **(B)** Quantification of myelinated axons in the femoral sensory branch indicates a significant difference ($P = 0.015$) in the HOM sensory axons (693 ± 38.3 , $n = 6$) compared with WT (802 ± 12.3 , $n = 4$) or heterozygous (816 ± 46 , $n = 7$) at 8 weeks of age. **(C)** Quantification of myelinated axons in the femoral motor branch indicates significant ($P < 0.0001$) degeneration in the HOM axons (376 ± 23.9 , $n = 8$) compared with WT (570 ± 10.9 , $n = 4$) or heterozygous (569 ± 20.7 , $n = 7$) at 8 weeks of age. **(D)** Quantification of myelinated axons in the femoral sensory branch indicates a significant difference ($P = 0.015$) in the HOM sensory axons (706.7 ± 39.9 , $n = 15$) compared with WT (881.6 ± 34.2 , $n = 12$) at 16 weeks of age. **(E)** Quantification of myelinated axons in the femoral motor branch indicates significant ($P < 0.0001$) degeneration in the HOM axons (404.8 ± 34 , $n = 6$) compared with WT (597.9 ± 62.33 , $n = 8$) at 16 weeks of age. **(F)** Axon diameters of the femoral sensory nerves were analyzed via the Tukey's multiple comparison's test, and found that in bin sizes $2\text{--}4 \mu\text{M}$, there were significantly fewer axons in homozygotes than WT and heterozygote mice, respectively ($P = 0.0486$, $P = 0.0351$) ($2\text{--}4 \mu\text{M}$, $+/+ = 632.1 \pm 46.11$, $Y918C/+ = 578.1 \pm 109.7$, $Y918C/Y918C = 470.7 \pm 33.08$, $+/+$, $n = 7$, $Y918C/+$, $n = 7$, $Y918C/Y918C$, $n = 3$). **(G)** Axon diameters of the femoral motor nerves were analyzed via the Tukey's multiple comparison's test, and found that in bin sizes $4\text{--}6 \mu\text{M}$ and $6\text{--}8 \mu\text{M}$, there were significantly fewer axons in homozygotes than WT and heterozygote mice, respectively ($4\text{--}6 \mu\text{M}$: $P = 0.0063$, $P \leq 0.0001$; $6\text{--}8 \mu\text{M}$: $P = 0.0053$,

will be an important consideration as gene therapies and other treatment strategies are developed (26,27).

These models, though similar behaviorally and overtly, show nuanced differences at the histological and electrophysiological level further demonstrating a need to not only expand the range of IGHMBP2 models to display the full spectrum of human disease associated with IGHMBP2, but the importance of mutation location in phenotypically similar disease models. Future work with these models can help to determine if previously tested gene therapies in SMARD1 models would be equally effective in these less severe mouse models (26,27). Determining the therapeutic window will be critical, as many patients are identified after significant motor and sensory function deficits and degeneration have begun. These mice show we can model the entire phenotypic spectrum of IGHMBP2-related diseases and will allow greater resolution to examine the pathomechanisms involved.

Materials and Methods

CRISPR-Cas9 mutagenesis

The C57BL/6 J-Ighmbp2^{em1Cx}/Cx (herein E365del, stock #28670, The Jackson Laboratory) and C57BL/6 J-Ighmbp2^{em5Cx}/Cx (herein Tyr918Cys, stock #33393, The Jackson Laboratory) strains were generated via CRISPR-Cas9 mutagenesis performed by cytoplasmic microinjection of C57BL/6 J zygotes with 100 ng/ μ L Cas9 mRNA and 50 ng/ μ L of sgRNA (ACCACATCAAAGTAGTCCTCAGG) targeting exon 8 of Ighmbp2 for E365del or 50 ng/ μ L sgRNA (1: CTTACAGCAGATGGTGGCTG; 2: CCCTCACTTCAGGCAGATGG) and 20 ng/ μ L donor oligo (GCTGACAACACCTGTAGCTTCTCAAGTGTCTCGGCCAGCACCACCTCTGGGCCA GTTCTGCATGCACTGTAGCCACCGTGTGCCTCAGCCACCATCTGCCGAAGTGAG GGCCCTTCTGGAC). Mosaic founder mice identified as carrying a mutation of interest in the targeted region were backcrossed to C57BL/6J. Resulting N1 progeny identified as carrying the mutation were further backcrossed to C57BL/6J to establish the colony and breed away from any potential off-target mutation. After a minimum of two backcrosses, mice were crossed in a sibling by sibling mating (N2F1) in order to assess animals carrying HOM mutation of interest.

Mouse strains and genotyping

All mouse husbandry and procedures were reviewed and approved by the Institutional Animal Care and Use Committee at The Jackson Laboratory, and were carried out according to the NIH Guide for Care and Use of Laboratory Animals. Mice were bred and maintained under standard conditions. Tail or ear tissue was lysed in proteinase K at 55°C overnight and extracted gDNA was used to determine genotype. Genotyping for C57BL/6 J-Ighmbp2^{em1Cx}/Cx (JAX stock #28670) was performed via PCR using the following primers: forward primer specific to the wild type allele: 5'- TGC TGC CTG AGG ACT ACT T -3'; forward primer specific to the mutant em1 (L365del) allele: 5'- TGA AGC TGC TGC CTG ACT-3' and reverse primer common for both alleles (i8r3) 5'- AGGACTAACAGCCACACTGC-3'. Genotyping for C57BL/6 J-Ighmbp2^{em5Cx}/Cx (JAX stock #33393) was performed

via PCR forward primer: 5'- ACC ACT CTG GC CAG TTC T -3' and reverse primer 5'- CCC ACA TC TCC AGA AGG -3' with a 5HEX-probe for the WT 5'-CCA CCG CTA CTG CCT CAG -3' and a 6-FAM probe for mutant allele 5'-CAC CGC TGC TGC CTC A -3'.

Functional and behavioral assays

von Frey assessment

Mechanical allodynia was assessed by stimulating the plantar surface of the mouse's hindpaw and measuring the latency to paw withdrawal. Mice are first habituated to the testing room for a 60 min period minimum and then allowed to habituate to the Plexiglas testing cubical for 30 min. The touch stimulator is moved to the paw for 1–2 s using the up-down method (28). Between presentations of stimuli an interval of several seconds is used in order to allow a response to the prior stimuli. Von Frey-type monofilaments with binding forces of 0.02, 0.07, 0.16, 0.41, 1.0, 2.24, 5.5 g are applied successively to the plantar surface until a response is observed. The threshold force required to elicit a withdrawal at least 50% of the time is determined. Males and females were analyzed separately and compared and found no significant sex impact on von Frey assay.

Hot plate test

Hot plate test was utilized to evaluate thermal pain reflexes. Mice were habituated to the testing room for a minimum of 30 min. A hot plate (Harvard apparatus LE7406) was maintained at 52 \pm 2°C. Mice are placed into the cylinder and observed, with latency recorded to the first instance of paw withdrawal, including jumping, hind paw lick, paw shack or flutter to the nearest 0.1 s by a trained observer, who was blind to the subject's genotype. Maximum time allowed was 30 s, after which the mouse was removed. Two trials were performed per mouse with an intertrial interval of 30 s. Males and females were analyzed separately and compared and found no significant sex impact.

Adhesive tape removal test

To test both somatosensory and fine motor function an adhesive tape removal test was employed. Performance is assessed by measuring the time necessary to both sense and remove the adhesive. Briefly, the mice are acclimated to the procedure room for a minimum 60 min period and then acclimated to the observation arena for 10 min prior to adhesive placement. Mice are gently restrained and adhesive label tape (Avery 0.25"–0.75" diameter) is applied to the central forehead area. The latency to first contact with the tape, as well as the total time to remove is recorded. Maximum time allowed is 5 min. Males and females were analyzed separately and compared and found no significant sex impact.

Wire hang assay

Inverted wire hang assay was used to assess motor function starting at 2 weeks of age. Mice were placed on top of a wire mesh, which was then inverted allowing the mouse to hang suspended from it for a maximum of 60 s, and the latency to fall was measured. Mice were allowed to rest for a minimum of 5 min

P = 0.0001) (4–6 μ M, +/+ = 147.5 \pm 16.83, Y918C/+ = 161.5 \pm 7.969, Y918C/Y918C = 96 \pm 5.727, 6–8 μ M, +/+ = 116.5 \pm 23.49, Y918C/+ = 142.7 \pm 10.33, Y918C/Y918C = 50.83 \pm 14.15, +/+, n = 8, Y918C/+, n = 6, Y918C/Y918C, n = 6). (H) NCV was significantly reduced in HOM (n = 8, 25.9 \pm 2.9, P < 0.0001) and heterozygous (n = 8, 30.5 \pm 1.9, P = 0.0007) mice compared with WT littermates (n = 12, 36.3 \pm 3.4), with heterozygous showing an intermediate phenotype, at 8 weeks of age. (I) NMJs were quantified as occupied, partially occupied or unoccupied. The percent of junctions that were unoccupied was significantly different in HOM compared with WT evident by 16 weeks of age (P = 0.0001) (n = 5–7 per time point). (J) G-ratios (ratio of myelin thickness to axon diameter) of HOM (0.159 \pm 0.076, n = 7), heterozygous (0.153 \pm 0.049, n = 6) and WT (0.150 \pm 0.086, n = 3) showed no significant difference.

before repeating the test. The average of two tests was recorded per time-point. Where sex is not indicated, mice are presented as mixed sex, as prior analysis determined no significant sex impacts.

Rotarod test

Rotarod was employed to test motor coordination of mice at 14 weeks of age. An Ugo Basile rotarod was utilized; briefly, the subject was placed on a fixed speed rod rotating at 4 rpm that increased linearly to a maximum of 40 rpm over 300 s. Mice were given three successive trials, with about a 1 min intertrial interval. Males and females were analyzed separately and compared and found no significant sex impact.

Voluntary homecage wheel running

Mice were individually housed with low profile running wheels with a wireless transmitter (Med Associates Inc, ENV-047). Running wheel rotations were measured in 1-h bins to allow for distance traveled (sum of rotations) calculated per mouse each night. Average rotations were calculated per mouse for each tracked night. Average speed while active was calculated by isolating the dark hour intervals where activity was measured, and averaging the number of rotations over the 12 h dark period.

Nerve conduction analysis

Sciatic NCV was assessed as previously described (29). Briefly, sciatic NCV was determined by measuring the latency of compound motor action potentials recorded in the muscle of the right rear paw. Mice were anesthetized with 1.5–2.0% isoflurane and placed on a thermostatically regulated heat pad in order to properly maintain normal body temperature. Action potentials were evoked via subcutaneous stimulation at the sciatic notch and at the ankle. The reference electrode was placed in the skin between the 4th and 5th digits, while the active recording needle electrode was inserted in the center of the paw. To calculate velocity, the distance between the stimulation points was measured and divided by the proximal minus distal latencies.

Grip strength test

To test for grip strength a commercially available grip strength meter (Bioseb) was used to measure forelimb and combined fore/hindlimb grasp strength as an indicator of neuromuscular function. For measurements a wire grid was coupled to a strain gage, which measure peak force (kg) the mouse was lowered gently toward the wire grid until it instinctively grasped the bar, with both front paws only for forepaw measurements and all four paws for the combined. Animal was gently and firmly pulled from the grid until it released, measuring the peak force in kg for a total of six consecutive trials (three forepaw only, three combined). An average over all three of each type of trial was calculated.

In vivo torque recording

Mice were anesthetized with isoflurane in O₂ (5% induction, 2–3% maintenance) and the hair was trimmed off the lower limb. Mice were placed supine on a homeothermic platform (32°C) with the left knee immobilized in a clamp employing a 25 gage needle pressed against the lateral, proximal tibia. The tibia was positioned horizontally, orthogonal to the left hind paw that rested in a foot plate on a micromanipulator (300C-FP, Aurora Scientific, Ontario, Canada). Tape (3M Transpore) was used to secure the dorsal surface of the paw to the foot plate. The axis of the foot plate was attached to a torque sensor (605A, Aurora Scientific) and measures the torque of the dorsiflexion of the foot when

the tibialis anterior muscle contracts. Data was recorded with the DMC software (Aurora Scientific) and analyzed with the DMA software (Aurora Scientific). Muscle contractions were elicited by electrical stimulation (701C, Aurora Scientific) with a pair of stainless steel electrodes. Duration of anesthesia was less than 15 min. Torque responses were recorded at increasing frequencies at 10 s intervals: a single pulse (T0 or twitch), 10, 30, 50, 80, 120 and 150 Hz, with each stimulation applied for 300 ms. The maximum torque obtained for each stimulation frequency was used to produce the force-frequency curves.

Echocardiography

Mice were anesthetized with 5% isoflurane mixed with 100% oxygen at 1.0 l/min flow and then maintained under anesthesia with 1.5% isoflurane/oxygen flow. Ophthalmic ointment was placed on the eyes to prevent drying of the cornea while the mouse was anesthetized and tested. Mice were placed on a thermostatically controlled heated platform, where isoflurane anesthesia was maintained by delivery through a close fitting face mask. A heating lamp was also used to keep the heart rate and body temperature constant at physiological status during echocardiography. During the examination, the animal's heart rate was monitored through the use of an electrocardiograph. The mouse's heart rate and body temperature were monitored continuously during the scanning. Fur was removed from the ventral surface of the mouse torso with clippers and Nair (Church & Dwight, Ewing, NJ).

Histology

Analysis of femoral nerves

Motor and sensory branches of the femoral nerve were dissected and fixed overnight as previously described (30). For preliminary data, myelinated axon count and diameter analyses, images were captured using a Nikon Eclipse E600 microscope with a 40× objective. The total number of myelinated axons in each nerve was counted using an automated method in ImageJ with manual confirmation as previously described (29). Briefly, with ImageJ software, the Threshold function was adjusted in order to only highlight axoplasm on whole nerve sections, and Analyze particle function was then used to quantify the number of myelinated axons and areas of each nerve. The diameter was determined from axonal area. Images of large nerves that could not be captured as a single image at 40× magnification were generated as montages to show the whole nerve, using the ImageJ Stitching Grid/Pairwise plugin (31). For 19 week femoral motor and sensory branch data, slides were scanned using a NanoZoomer 2.0 (Hamamatsu) at 40× magnification. Whole nerve representative images were taken from 20× digital magnification using NDP.view2 software (Hamamatsu) and if needed stitched together using ImageJ Stitching Grid/Pairwise (31). For quantification ImageJ software was utilized as with the preliminary data and for analyze particles size was set at 20-infinity pixel units with circularity threshold of 0.40–1.00.

G-ratios

Femoral motor axons of 19 week-old WT, heterozygous and HOM Y918C animals were evaluated at 80 kV using a JEOL JM-1230 transmission electron microscope (JEOL, Tokyo, Japan) and images collected with an AMT 2K digital camera (Advanced Microscopy Techniques, Woburn, MA.) with a 4000× objective. Myelin thickness and axon diameter of 100 axons per nerve were collected and g-ratios were calculated by dividing the myelin thickness by

the inner axon diameter by the outer axon diameter for each respective axon.

NMJ visualization and quantification

Tissue (MG & soleus) was dissected and fixed for 2 h in cold 2% paraformaldehyde/PBS. The samples were then incubated in blocking solution [2.5% BSA (Sigma-Aldrich) and 1% Triton-X 100 (Sigma-Aldrich) in PBS] for 1 h before they were gently teased apart and pressed between two glass slides using a binder clip for 15 min at 4°C. Nerves were visualized with the transgenic-EYFP. Acetylcholine receptors (AChRs) were visualized by staining with 1:1000 α -bungarotoxin conjugated with Alexa-Fluor 594 (Invitrogen, Carlsbad, CA), incubated at room temperature on a rocker in blocking solution for 2 h. Postincubation samples were rinsed three times and washed at least four times for 15 min each. Samples were mounted in gelvatrol (<http://cshprotocols.cshlp.org/content/2006/1/pdb.rec10252.short>). Occupancy of 50 or greater randomly selected NMJs were scored blinded to genotype on a Nikon E600 fluorescence microscope. Full occupancy of NMJ was defined as when presynaptic nerve staining fully overlaid with AChR, partial occupancy as when positive for AChR but only partially stained for presynaptic nerve and denervation as when positive for AChR but negative for presynaptic nerve staining. Images were obtained on a Leica SP8 laser-scanning confocal microscope with a 63 \times objective lens. Z stacks were collapsed into projected images and merged using ImageJ (NIH, <http://rsb.info.nih.gov/ij/>).

H&E staining

Mice were euthanized and right hindlimb was extracted and post-fixed in Bouin's fixative. Whole hindlimbs were cross-sectioned through the middle portion of lower and upper legs. The sectioned tissues were then paraffin-embedded, sectioned, mounted and stained with hematoxylin and eosin for light microscopic analysis according to standard histological procedures. For the E365del representative images slides were scanned using a NanoZoomer 2.0 (Hamamatsu) at 40 \times magnification. Representative images were taken from the MG region of the lower leg, and whole lower limb using NDP.view2 software (Hamamatsu). For Y918C representative images slides were imaged at 60 \times magnification on a Nikon Eclipse E600 microscope and images were stitched if needed in FIJI using Stitching Grid/Pairwise plugin (31).

Trichrome staining

Mice were euthanized with CO₂ and perfused with HBSS buffer (ThermoFisher). The heart was carefully removed and placed in 60 mM KCl while still beating to synchronize the contractile phase for 5 min before fixing in 4% PFA overnight at 4°C. They were then embedded in paraffin and sectioned coronally around the mid-line of the heart and stained with trichrome. Representative images were taken from the upper portion of the left ventricle on Nikon Eclipse E600 microscope at 60 \times magnification.

TaqMan™ gene expression analysis

Whole spinal cords were collected at 2 weeks of age and snap frozen on liquid. Frozen tissue was homogenized using a PowerGen 125 homogenizer (Fisher Scientific) in TRIzol™ reagent (Invitrogen #15596026). After the addition of chloroform and phase separation, the aqueous phase was transferred to a miRNEasy Kit column (Qiagen cat#217004) and processed according to the kit protocol with the addition of a DNase treatment (Qiagen cat#79254) on the column. RNA quantity was measured using a NanoDrop (ThermoFisher Scientific), and 1 μ g

of total RNA was used to synthesize cDNA with a SuperScript® III First-Strand Synthesis Kit (Invitrogen #18080-0051) and random hexamers. Ighbmp2 was measured using a TaqMan™ gene expression assay (Applied Biosystems Mm00456315_m1 assay) and normalized against GAPDH expression (Applied Biosystems Mm99999915_g1 assay) in the same reaction. Data was graphed using Prism 7 software (GraphPad) and a two-way ANOVA with Tukey's multiple comparison test was used to determine significant differences.

Statistical analyses

Statistical tests were performed using GraphPad's Prism 7 software. A threshold of $P < 0.05$ was considered significant. Significance was determined using a one or two-way ANOVA and a post-hoc Tukey test for individual difference when appropriate. For data with males and females combined, it was determined that there was no sex dependent difference with a one-way ANOVA. The use of other tests are noted in the legends. Results are presented as means \pm SD.

Supplementary Material

Supplementary Material is available at HMG online.

Acknowledgements

The authors would like to acknowledge the contribution of the following people and cores at The Jackson Laboratory for their expert assistance with the work described in this publication: Bob Schneider, Blaine Pattavina and Genetic Resource Science group, Dave Schroeder, Jenn Stauffer, Pete Finger, Histopathology Core, Rick Maser, Rebecca Boumil and Genetic Engineering Technologies, Rachel Sands and the Microscopy Core and the Neurobehavioral Phenotyping Service.

Conflict of Interest statement: None declared.

Funding

National Institutes of Health (R01 NS102414 to G.A.C. and R24 NS098523 to R.W.B.); Sims Family Fund (to G.A.C.).

References

- Skre, H. (1974) Genetic and clinical aspects of Charcot-Marie-Tooth's disease. *Clin. Genet.*, **6**, 98–118.
- Timmerman, V., Strickland, A.V. and Züchner, S. (2014) Genetics of Charcot-Marie-Tooth (CMT) disease within the frame of the human genome project success. *Genes (Basel)*, **5**, 13–32.
- Laurá, M., Pipis, M., Rossor, A.M. and Reilly, M.M. (2019) Charcot-Marie-Tooth disease and related disorders, an evolving landscape. *Curr. Opin. Neurol.*, **32**, 641–650.
- Yong, K.J., Milenic, D.E., Baidoo, K.E. and Brechbiel, M.W. (2014) Impact of ??-targeted radiation therapy on gene expression in a pre-clinical model for disseminated peritoneal disease when combined with paclitaxel. *PLoS One*, **9**, e108511.
- Martin, P.B., Hicks, A.N., Holbrook, S.E. and Cox, G.A. (2020) Overlapping spectrums: the clinicogenetic commonalities between Charcot-Marie-Tooth and other neurodegenerative diseases. *Brain Res.*, **1727**, 146532.
- Gonzalez, M.A., Feely, S.M., Speziani, F., Strickland, A.V., Danzi, M., Bacon, C., Lee, Y., Chou, T.F., Blanton, S.H., Wehl, C.C.,

- Zuchner, S. and Shy, M.E. (2014) A novel mutation in VCP causes Charcot-Marie-Tooth Type 2 disease. *Brain*, **137**, 2897–2902.
7. James, P.A., Cader, M.Z., Muntoni, F., Childs, A.M., Crow, Y.J. and Talbot, K. (2006) Severe childhood SMA and axonal CMT due to anticodon binding domain mutations in the GARS gene. *Neurology*, **67**, 1710–1712.
 8. Bennett, C.L., Dastidar, S.G., Ling, S.C., Malik, B., Ashe, T., Wadhwa, M., Miller, D.B., Lee, C., Mitchell, M.B., van Es, M.A. et al. (2018) Senataxin mutations elicit motor neuron degeneration phenotypes and yield TDP-43 mislocalization in ALS4 mice and human patients. *Acta Neuropathol.*, **136**, 425–443.
 9. Wagner, J.D., Huang, L., Tetreault, M., Majewski, J., Boycott, K.M., Bulman, D.E., Care4Rare Canada Consortium, Dymont, D.A. and McMillan, H.J. (2015) Autosomal recessive axonal polyneuropathy in a sibling pair due to a novel homozygous mutation in IGHMBP2. *Neuromuscul. Disord.*, **25**, 794–799.
 10. Cottenie, E., Kochanski, A., Jordanova, A., Bansagi, B., Zimon, M., Horga, A., Jaunmuktane, Z., Saveri, P., Rasic, V.M., Baets, J. et al. (2014) Truncating and missense mutations in IGHMBP2 cause Charcot-Marie tooth disease type 2. *Am. J. Hum. Genet.*, **95**, 590–601.
 11. Cox, G.A., Mahaffey, C.L. and Frankel, W.N. (1998) Identification of the mouse neuromuscular degeneration gene and mapping of a second site suppressor allele. *Neuron*, **21**, 1327–1337.
 12. Guenther, U.P., Handoko, L., Laggenbauer, B., Jablonka, S., Chari, A., Alzheimer, M., Ohmer, J., Plöttner, O., Gehring, N., Sickmann, A. et al. (2009) IGHMBP2 is a ribosome-associated helicase inactive in the neuromuscular disorder distal SMA type 1 (DSMA1). *Hum. Mol. Genet.*, **18**, 1288–1300.
 13. Maddatu, T.P., Garvey, S.M., Schroeder, D.G., Hampton, T.G. and Cox, G.A. (2004) Transgenic rescue of neurogenic atrophy in the nmd mouse reveals a role for Ighmbp2 in dilated cardiomyopathy. *Hum. Mol. Genet.*, **13**, 1105–1115.
 14. Grohmann, K., Schuelke, M., Diers, A., Hoffmann, K., Lucke, B., Adams, C., Bertini, E., Leonhardt-Horti, H., Muntoni, F., Ouvrier, R. et al. (2001) Mutations in the gene encoding immunoglobulin mu-binding protein 2 cause spinal muscular atrophy with respiratory distress type 1. *Nat. Genet.*, **29**, 75–77.
 15. Liu, L., Li, X., Hu, Z., Mao, X., Zi, X., Xia, K., Tang, B. and Zhang, R. (2017) IGHMBP2-related clinical and genetic features in a cohort of Chinese Charcot-Marie-Tooth disease type 2 patients. *Neuromuscul. Disord.*, **27**, 193–199.
 16. Grohmann, K., Rossoll, W., Kobsar, I., Holtmann, B., Jablonka, S., Wessig, C., Stoltenburg-Didinger, G., Fischer, U., Hübner, C., Martini, R. and Sendtner, M. (2004) Characterization of Ighmbp2 in motor neurons and implications for the pathomechanism in a mouse model of human spinal muscular atrophy with respiratory distress type 1 (SMARD1). *Hum. Mol. Genet.*, **13**, 2031–2042.
 17. Luan, X., Huang, X., Liu, X., Zhou, H., Chen, S. and Cao, L. (2016) Infantile spinal muscular atrophy with respiratory distress type I presenting without respiratory involvement: novel mutations and review of the literature. *Brain Dev.* **38**, 685–689.
 18. Shababi, M., Smith, C.E., Kacher, M., Alrawi, Z., Villalón, E., Davis, D., Bryda, E.C. and Lorson, C.L. (2019) Development of a novel severe mouse model of spinal muscular atrophy with respiratory distress type 1, FVB-nmd. *Biochem. Biophys. Res. Commun.*, **520**, 341–346.
 19. Smith, C.E., Lorson, M.A., Ricardez Hernandez, S.M., Al Rawi, Z., Mao, J., Marquez, J., Villalón, E., Keilholz, A.N., Smith, C.L., Garro-Kacher, M.O. et al. (2021) The Ighmbp2D564N mouse model is the first SMARD1 model to demonstrate respiratory defects. *Hum. Mol. Genet.* **31**, 1293–1307.
 20. Maddatu, T.P., Garvey, S.M., Schroeder, D.G., Zhang, W., Kim, S., Nicholson, A.I., Davis, C.J. and Cox, G.A. (2005) Dilated cardiomyopathy in the nmd mouse, transgenic rescue and QTLs that improve cardiac function and survival. *Hum. Mol. Genet.*, **14**, 3179–3189.
 21. Yuan, J.H., Hashiguchi, A., Yoshimura, A., Yaguchi, H., Tsuzaki, K., Ikeda, A., Wada-Isoe, K., Ando, M., Nakamura, T., Higuchi, Y. et al. (2017) Clinical diversity caused by novel IGHMBP2 variants. *J. Hum. Genet.* **62**, 599–604.
 22. Guenther, U.P., Handoko, L., Varon, R., Stephani, U., Tsao, C.Y., Mendell, J.R., Lützkendorf, S., Hübner, C., von Au, K., Jablonka, S. et al. (2009) Clinical variability in distal spinal muscular atrophy type 1 (DSMA1): determination of steady-state IGHMBP2 protein levels in five patients with infantile and juvenile disease. *J. Mol. Med.*, **87**, 31–41.
 23. Joseph, S., Robb, S.A., Mohammed, S., Lillis, S., Simonds, A., Manzur, A.Y., Walter, S. and Wraige, E. (2009) Interfamilial phenotypic heterogeneity in SMARD1. *Neuromuscul. Disord.*, **19**, 193–195.
 24. Hamilton, M.J., Longman, C., O'Hara, A., Kirkpatrick, M. and McWilliam, R. (2015) Growing up with spinal muscular atrophy with respiratory distress (SMARD1). *Neuromuscul. Disord.*, **25**, 169–171.
 25. Lim, S.C., Bowler, M.W., Lai, T.F. and Song, H. (2012) The Ighmbp2 helicase structure reveals the molecular basis for disease-causing mutations in DMSA1. *Nucl. Acids Res.*, **40**, 11009–11022.
 26. Nizzardo, M., Simone, C., Rizzo, F., Salani, S., Dametti, S., Rinchetti, P., Del Bo, R., Foust, K., Kaspar, B.K. and Bresolin, N. (2015) Gene therapy rescues disease phenotype in a spinal muscular atrophy with respiratory distress type 1 (SMARD1) mouse model. *Sci. Adv.*, **13**, 1–10.
 27. Shababi, M., Feng, Z., Villalón, E., Sibigtroth, C.M., Osman, E.Y., Miller, M.R., Williams-Simon, P.A., Lombardi, A., Sass, T.H., Atkinson, A.K. et al. (2016) Rescue of a mouse model of spinal muscular atrophy with respiratory distress type 1 (SMARD1) by AAV9-IGHMBP2 is dose dependent. *Mol. Ther.*, **24**, 855–866.
 28. Chaplan, S.R., Bach, F.W., Pogrel, J.W., Chung, J.M. and Yaksh, T.L. (1994) Quantitative assessment of tactile allodynia in the rat paw. *J. Neurosci. Methods*, **53**, 55–63.
 29. Bogdanik, L.P., Sleigh, J.N., Tian, C., Samuels, M.E., Bedard, K., Seburn, K.L. and Burgess, R.W. (2013) Loss of the E3 ubiquitin ligase LRSAM1 sensitizes peripheral axons to degeneration in a mouse model of Charcot-Marie-Tooth disease. *Dis. Model. Mech.*, **6**, 780–792.
 30. Seburn, K.L., Nangle, L.A., Cox, G.A., Schimmel, P. and Burgess, R.W. (2006) An active dominant mutation of glycyl-tRNA synthetase causes neuropathy in a Charcot-Marie-Tooth 2D mouse model. *Neuron*, **51**, 715–726.
 31. Preibisch, S., Saalfeld, S. and Tomancak, P. (2009) Globally optimal stitching of tiled 3D microscopic image acquisitions. *Bioinformatics*, **25**, 1463–1465.